

Flux-driven quantum spin liquids in kagome optical lattices

Hoi-Yin Hui,^{1,*} Mengsu Chen,¹ Sumanta Tewari,² and V.W. Scarola^{1,†}

¹*Department of Physics, Virginia Tech, Blacksburg, Virginia 24061, USA*

²*Department of Physics and Astronomy, Clemson University, Clemson, South Carolina 29634, USA*

Quantum spin liquids (QSLs) define an exotic class of quantum ground states where spins are disordered down to zero temperature and are characterized by macroscopic entanglement and fractionalized excitations. We propose a route to QSLs in kagome optical lattices using applied flux. An optical flux lattice can be applied to induce a uniform flux and chiral three-spin interactions that drive the formation of a gapped chiral spin liquid. A different approach based on recent experiments using laser assisted tunneling and lattice tilt implements a staggered flux pattern which can drive a gapless spin liquid with symmetry protected nodal lines. Our proposal therefore establishes kagome optical lattices with effective flux as a powerful platform for exploration of QSLs.

QSLs defy conventional paradigms of magnetic ordering known from Landau theory but may nonetheless offer explanations for strongly correlated phenomena observed in some materials [1, 2]. Frustration is known to favor certain types of QSLs. Kagome lattice models of spins in particular serve as a central archetype hosting a broad array of QSL states. It is now well established that ground states arising from the standard antiferromagnetic Heisenberg interaction ($\mathbf{S}_i \cdot \mathbf{S}_j$, where \mathbf{S}_i is the usual spin operator at a site i) on a kagome lattice can be driven into exotic spin liquids when certain three-spin interactions [$\mathbf{S}_i \cdot (\mathbf{S}_j \times \mathbf{S}_k)$] are added to the Heisenberg interaction [3–8].

When the three-spin interaction is added uniformly everywhere to the kagome lattice, a chiral spin liquid (CSL) arises [4–6]. A CSL is related to a bosonic Laughlin state [3, 9], and, as such, derives some of the same properties. The CSL is: a topologically ordered ground state and is therefore two-fold degenerate on the torus; It possesses chiral edge modes; Derives from flux attachment in effective Chern-Simons theories [7]; And furthermore, the CSL hosts exotic anyon excitations, whereby braiding of anyons changes the many-body wavefunction by a non-trivial phase [10, 11]. Identifying such exotic braid statistics in the laboratory remains a key goal of quantum many-body physics [11].

Prospects for driving kagome antiferromagnets into the CSL remains daunting and rare in the published literature. Recent works with ultracold atoms placed in optical lattices [12, 13] show promise because not only are kagome lattices possible [14, 15], but also temperatures low enough to realize antiferromagnetic order derived from super exchange between fermionic atoms have recently been realized [16] with atomic gas microscopes [17–34]. One recent idea suggests that a CSL may be realizable in systems of polar molecules using long-ranged dipolar interactions in optical lattices [35]. In this paper we examine a very different approach based on more common short-ranged interactions of fermionic atoms in the presence of tunable fluxes.

We model fermionic atoms placed in kagome optical lattices with flux. Effective flux in optical lattices can be realized in a variety of ways [36–45]. We show that an optical flux lattice [38] can be used to generate a sufficient amount of flux to drive virtual currents in an underlying Hubbard model

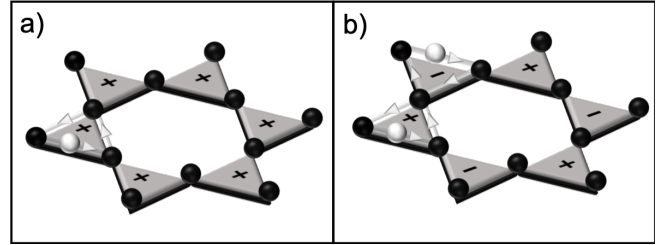


FIG. 1. Schematic of one fermion per site (black spheres) on a kagome lattice. The white spheres denote virtual current driven by flux passing through the lattice. The plus and minus signs denote the sign of the flux captured by the virtual currents. Panel a (b) shows a uniform (staggered) flux pattern. In the Heisenberg limit of a Hubbard model, virtual currents encircling flux lead to chiral three-spin terms that drive spin liquids.

[46–48]. Fig. 1a shows one fermion per site in the Mott limit. Ordinary hopping is prevented but virtual hops around triangles can capture flux to drive three spin terms needed to enhance the CSL. The equivalent amount of flux for such terms in a solid with an $\sim 1 \text{ \AA}$ inter-atomic spacing would require large magnetic fields, $\sim 10^4 \text{ T}$. We will therefore show that an optical flux lattice in a kagome optical lattice offers a more direct route to the CSL than what is achievable in solids with ordinary magnetic field strengths.

We also model effective flux generated by laser assisted tunneling combined with a potential tilt as first implemented in square optical lattices [43, 44]. When examining this setup in a kagome optical lattice we find that the effective flux pattern is staggered (Fig. 1b) instead of uniform as one might expect. We speculate that this flux pattern may be able to drive an interesting gapless spin liquid recently discovered numerically [8] to host symmetry protected nodal lines and may thus offer a platform to study gapless spinon surfaces [49–52]. Overall, our findings show that flux applied to kagome optical lattices offers a powerful tool to study QSLs, in particular, the long sought chiral spin liquid, and a spin liquid with gapless spinon surfaces.

Hubbard model and kagome optical lattices: We consider fermionic alkali atoms equally populating two pseudo-spin states derived from hyperfine levels and loaded into a kagome

optical lattice deep enough to realize the Hubbard limit [14, 15, 53]:

$$H^\alpha = H_0^\alpha + U \sum_i n_{i\uparrow} n_{i\downarrow}, \quad (1)$$

where the second term is a repulsive Hubbard interaction derived from the s -wave scattering between atoms in spin states $\sigma \in \{\uparrow, \downarrow\}$. Here $n_{i\sigma} = a_{i\sigma}^\dagger a_{i\sigma}$ is defined in terms of dressed fermion annihilation ($a_{j\sigma}$) and creation ($a_{i\sigma}^\dagger$) operators at the site \mathbf{R}_i . The first term is a single particle hopping term:

$$H_0^\alpha = - \sum_{\langle ij \rangle} t_{ij}^\alpha a_{i\sigma}^\dagger a_{j\sigma}, \quad (2)$$

with nearest neighbor hopping matrix elements t_{ij}^α .

We will discuss two strategies to realize effective magnetic fields strong enough to drive Mott insulating states toward QSLs in kagome optical lattices. The strategies will lead to a uniform (Fig. 1a, $\alpha = \text{Un}$) and staggered (Fig. 1b, $\alpha = \text{St}$) flux patterns through triangles in the kagome lattice. The flux will be induced by effective gauge fields, \mathbf{A} , captured by a complex hopping via the Peierls transformation: $t_{ij}^\alpha = |t_{ij}| \exp(i\Phi_{ij}/\Phi_0)$, where the flux on a bond is $\Phi_{ij} = \int_{\mathbf{R}_i}^{\mathbf{R}_j} \mathbf{A} \cdot d\mathbf{r}$. The flux then leads to an Aharonov-Bohm phase difference as a particle tunnels around a triangle: $2\pi\Phi_\Delta/\phi_0$, where $\Phi_\Delta = \int_\Delta (\nabla \times \mathbf{A}) \cdot d^2\mathbf{r}$ is the flux through an upward pointing triangle in the kagome lattice (Φ_∇ is defined in the same way but for sites comprising downward pointing triangles). In the following we work in units $\hbar = a = q = 1$ where a is the lattice spacing and q is the effective charge so that $\Phi_0 = 2\pi$.

We now turn to interaction effects in the Heisenberg limit to study the role of our proposed flux patterns in driving QSLs. Eq. 1 is well approximated by spin models when there is one particle per site and for $t \ll U$. In this limit we can derive the spin model by expanding H^α in powers of t/U using $\exp(iK)H^\alpha \exp(-iK)$ where K is an operator that changes the number of doubly occupied sites [54]. Projecting into the limit of one particle per site we have [46, 47, 54]:

$$H^\alpha \approx J_H \sum_{\langle ij \rangle} \mathbf{S}_i \cdot \mathbf{S}_j + J_C \left[\sum_{ijk \in \Delta} \mathbf{S}_i \cdot (\mathbf{S}_j \times \mathbf{S}_k) + P_\alpha \sum_{ijk \in \nabla} \mathbf{S}_i \cdot (\mathbf{S}_j \times \mathbf{S}_k) \right] + \mathcal{O}(t^5/U^4) \quad (3)$$

where we have used the mapping: $\mathbf{S}_i = (1/2)a_{i\sigma}^\dagger \boldsymbol{\sigma}_{\sigma,\sigma'} a_{i\sigma'}$, with $\boldsymbol{\sigma}_{\sigma,\sigma'}$ the elements of the usual Pauli matrices. The first term is the usual antiferromagnetic Heisenberg term arising from 2 and 4 virtual hops along bonds: $J_H = 4t^2/U + \mathcal{O}(t^4/U^3)$. Here we assumed that the magnitude of the hopping on all bonds, t , is the same without loss of generality.

The three-spin terms in Eq. 3 arise from third order virtual hops around triangles but in the presence of an effective field. They are Hermitian, vanish on bi-partite lattices because of particle-hole symmetry, and are non-zero only in the presence of time-reversal symmetry breaking on individual triangles

due to effective fluxes: $J_C = (24t^3/U^2)|\sin(2\pi\Phi_{\Delta,\nabla}/\Phi_0)|$. In the following we seek routes to impose the maximum amount of flux through each triangle: $|\Phi_{\Delta,\nabla}| = \Phi_0/4$. The parameter P_α captures both the uniform flux case $P_{\alpha=\text{Un}} = 1$ ($\Phi_\Delta = \Phi_\nabla$) and the staggered flux case $P_{\alpha=\text{St}} = -1$ ($\Phi_\Delta = -\Phi_\nabla$). We now turn to proposals to realize both staggered and uniform fluxes, and therefore Eqs. 1 - 3, in optical lattices. *Uniform Flux:* Optical flux lattices [38] offer a straightforward route to implement a uniform effective flux in a kagome optical lattice. To generate effective flux, we assume an atom which has four near-degenerate hyperfine states. Each pair of states experiences a lattice potential leading to an effective spin in a potential. The dynamics of each atom leads to a Berry's phase which is equivalent to a flux passing through a closed loop.

We consider counter propagating lasers defining the usual kagome potential but for four hyperfine states so that for each pair of hyperfine states the single particle Hamiltonian becomes:

$$\tilde{H}_0^{\text{Un}} = \frac{\mathbf{p}^2}{2m} + V_L \sum_{l=1}^3 \left[\cos(\mathbf{k}_l \cdot \mathbf{r}) - \frac{1}{5} \cos(2\mathbf{k}_l \cdot \mathbf{r}) \right] \sigma_l, \quad (4)$$

where V_L is the lattice depth, $\mathbf{k}_1 = (0, 1)$, $\mathbf{k}_2 = (\sqrt{3}/2, -1/2)$, $\mathbf{k}_3 = (-\sqrt{3}/2, -1/2)$, and σ_l are the Pauli matrices. If the kinetic energy is much smaller than the gap of the second term, the ground state adiabatically follows the second term in a dressed state $\phi(\mathbf{r})$. Writing the ground eigenstate of the second term as $|\Psi\rangle^\dagger = (\phi_1(\mathbf{r}), \phi_2(\mathbf{r}))$ we assume that the ground state of this Hamiltonian is non-degenerate everywhere. Projecting to its lower band leads to an effective two-component Hamiltonian with the vector potential $\mathbf{A} = i \langle \Psi | \nabla_{\mathbf{r}} | \Psi \rangle$. where the effective magnetic flux density perpendicular to the plane of the lattice becomes $n_\phi \equiv (\nabla \times \mathbf{A}) \cdot \hat{z} / \Phi_0$.

The top panel of Fig. 2 plots the lowest energy of the potential term in Eq. 4, E_L , for a single spin. Here we see that minima correspond to a kagome lattice as expected. The bottom panel plots the flux density in the lattice. The flux density pattern shows that the flux piercing each triangle is the same, thus corresponding to Fig. 1a.

The flux through the lattice can be tuned to yield a complex hopping. Passing to the tight binding limit we assume that V_L is large enough to keep all atoms in the lowest band of the kagome lattice. Eq. 4 then becomes well approximated by Eq. 2 with complex hopping, $t_{ij} = t \exp(i\Phi_{ij}/\Phi_0)$, where t is real and the same for all bonds. The hoppings capture a uniform flux passing through all triangles in the kagome lattice ($\Phi_\Delta = \Phi_\nabla$). We have checked that the flux passing through triangles in Fig. 2 is maximized: $\text{Im}[t_{12}t_{23}t_{31}] = t^3 \sin(2\pi\Phi_\Delta/\Phi_0) = t^3 \sin(2\pi\Phi_\nabla/\Phi_0) \approx t^3$. This shows that an optical flux lattice can be tuned to yield a large uniform effective flux through a kagome optical lattice.

We now turn to interaction effects in the uniform flux case. Here we expect a gapped CSL. The three spin term on the kagome lattice, and therefore large $J_C \sim t^3/U^2$ in Eq. 3,

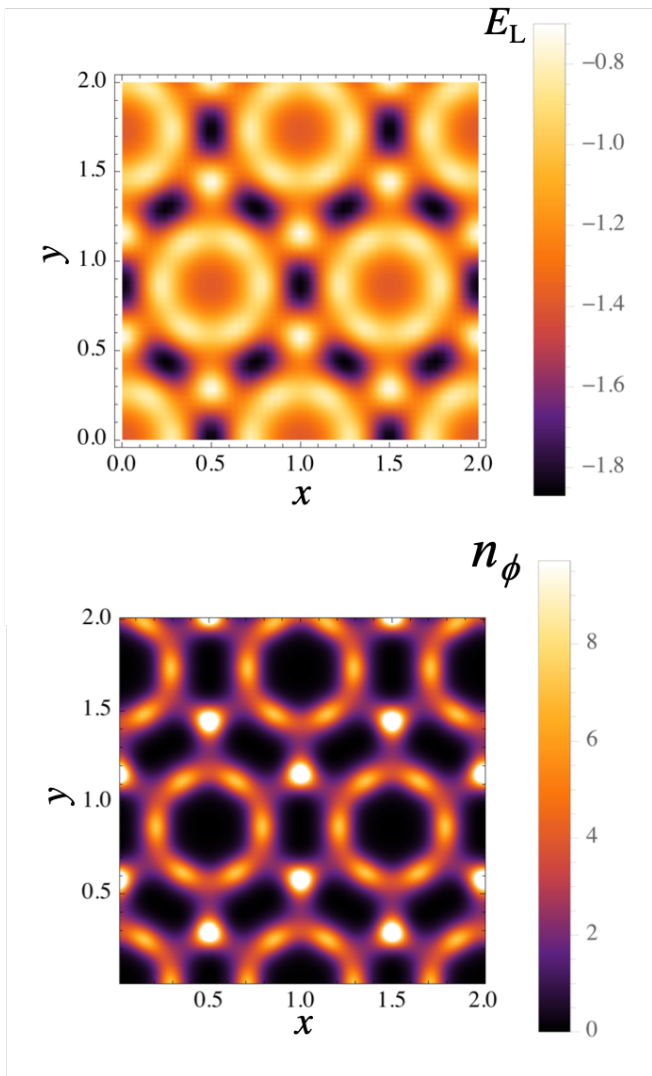


FIG. 2. Top: Lowest energy of the potential term in Eq. 4, E_L , used to implement the optical flux lattice for $V_L = 1$. The atoms sit at the energy minima (dark regions). Bottom: Same as the top but for the magnitude of the effective flux density, n_ϕ . The bright spots within triangles show that atoms experience a uniform flux through triangles (Fig. 1a).

strongly favors the CSL. But the derivation of Eq. 3 is most accurate in the perturbative limit, $t/U \ll 1$. We therefore search for an intermediate range of t/U which lies in the perturbative regime while still favoring the CSL. Large system size studies based on the density matrix renormalization group algorithm [55] find bounds on this parameter window in H_T^{Un} [6]. Here we study the robustness of the CSL over the entire parameter range using unbiased exact diagonalization for small system sizes. Exact diagonalization is applicable here since finite size effects remain below the gap.

Figure 3 plots the lowest energies of Eq. 3 for $P_{\alpha=Un} = 1$ as a function of the relative strength of each term for 18 spins with periodic boundary conditions. We have introduced θ

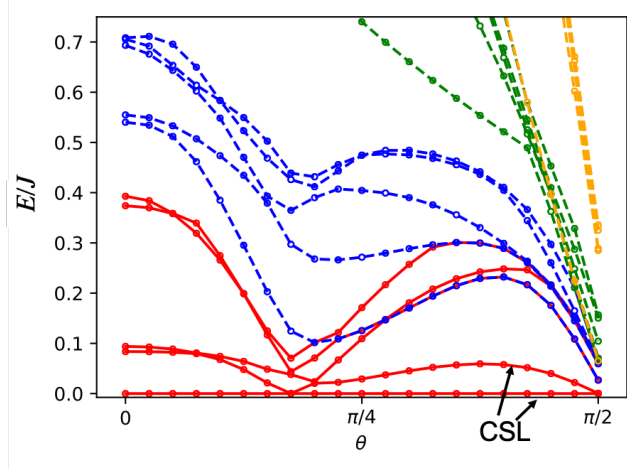


FIG. 3. Lowest energy eigenvalues of the spin model with uniform effective flux (Eq. 3 with $\alpha = Un$) for 18 spins in 2×3 unit cells with periodic boundaries. The lowest energy is set to zero. The strengths of the Heisenberg and chiral three-spin term are parameterized with $J_H = J \cos(\theta)$ and $J_C = J \sin(\theta)$, respectively. With this parameterization, we have $\tan(\theta) = 6t/U$ in the original Hubbard model. The right side of the graph is dominated by the three spin term where we see two ground states defining the CSL split by finite size effects. Different colors indicate different total spin sectors: red ($S_z = 0$), blue ($S_z = 1$), green ($S_z = 2$), and orange ($S_z = 3$).

so we can tune between the Heisenberg (left) and three-spin (right) limits in Eq. 3. The rightmost side of the graph shows a two-fold degenerate ground state (arrows), as expected for a CSL on a torus. There is a gap to a third state that remains robust for $\theta \gtrsim \pi/4$, i.e., $J_C/J_H \gtrsim 0.5$. In this regime we see that finite size effects and the Heisenberg term lift the exact degeneracy induced by the three-spin term at $\theta = \pi/2$. Nonetheless the CSL remains robust and is even somewhat enhanced by the two-spin term. Larger system size numerics [6] shows an even larger range of stability, $J_C/J_H \gtrsim 0.15$ in the thermodynamic limit. Returning to the original Hubbard parameters, this range of CSL stability, $t/U \gtrsim 0.16$ for 18 spins and $t/U \gtrsim 0.026$ in the thermodynamic limit, corresponds to parameters well within the assumption of the perturbative regime. This brings us to our central result: an optical flux lattice induces third-order virtual currents which in turn drive a CSL state in the Mott insulator regime of a Hubbard-kagome optical lattice.

Staggered Flux: We now discuss another method to introduce flux in a kagome optical lattice. The method is based on a scheme recently used to implement complex hopping terms in a square optical lattice [43, 44]. Fig. 4 shows a schematic of the kagome lattice with two external fields applied: a tilt and a moving lattice. The tilt can be applied using a variety of methods including a magnetic field or gravity. The moving lattice results from two additional Raman lasers applied perpendicular to the tilt.

The kinetic energy of the atoms under the applied fields

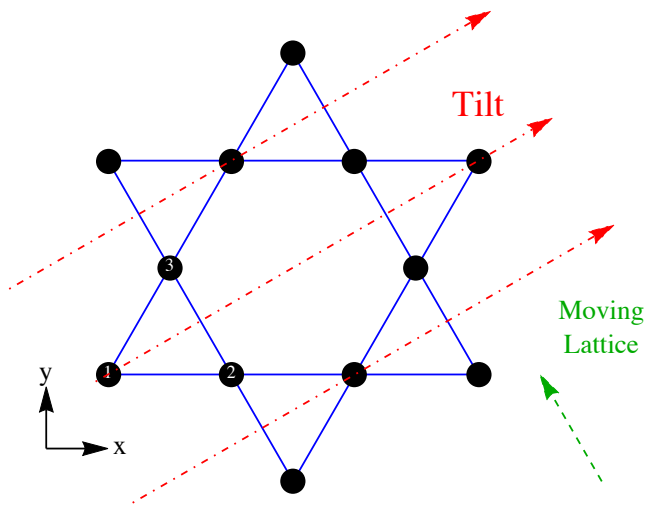


FIG. 4. Schematic of a kagome optical lattice with two additional fields applied to create a staggered effective flux (Fig. 1b). The arrows denote a uniform potential gradient (tilt) from a gravitational field, magnetic field, or another method. The green arrows denote the direction of the moving lattice created by additional Raman beams.

becomes a function of time τ :

$$\tilde{H}_0^{\text{St}} = -t \sum_{\langle ij \rangle \sigma} c_{i\sigma}^\dagger c_{j\sigma} + \sum_{i\sigma} \left[\vec{\Delta} \cdot \mathbf{R}_i + V(\mathbf{R}_i, \tau) \right] c_{i\sigma}^\dagger c_{i\sigma}, \quad (5)$$

where the annihilation and creation operators refer to undressed fermions (as in Eq. 2 but prior to the applied fields) in Wannier states localized at sites i and j . The second term results from the tilt field $\vec{\Delta} = \Delta [\hat{x} + (\sqrt{3}/3)\hat{y}] / 2$ such that $\vec{\Delta} \cdot \mathbf{R}_1 = 0$ and $\vec{\Delta} \cdot \mathbf{R}_2 = \vec{\Delta} \cdot \mathbf{R}_3 = \Delta/2$, where we assume the positions of the three sites in a unit cell are $\mathbf{R}_1 = \mathbf{0}$, $\mathbf{R}_2 = \hat{x}$ and $\mathbf{R}_3 = (1/2)\hat{x} + (\sqrt{3}/2)\hat{y}$. The last term is due to a moving lattice created by additional lasers added to the lasers defining the kagome potentials: $V(\mathbf{r}, \tau) = \Omega \sin(\mathbf{P} \cdot \mathbf{r} - \tau\Delta)$, where $\mathbf{P} = -(\pi/2)\hat{x} + (\sqrt{3}\pi/2)\hat{y}$ is the momentum of the moving lattice, such that $\mathbf{P} \cdot \vec{\Delta} = 0$, and $\mathbf{P} \cdot \mathbf{R}_3 = \mathbf{P} \cdot \mathbf{R}_1 + \pi/2 = \mathbf{P} \cdot \mathbf{R}_2 + \pi$. Here we have chosen an oscillation frequency that helps maximize flux and equalizes the hopping along all bonds.

We derive an effective model for the fermions under the applied fields where we tune Ω so that the magnitude of the hopping is the same on all bonds. By computing the Wannier functions in the presence of the tilt we find a Wannier-Stark effect which allows the moving lattice to generate a complex hopping [56]. We might expect the applied fields to yield an effective uniform flux (As in the square lattice [43, 44]), but we find [56] instead that the flux through the kagome lattice is staggered (Fig. 1b). Specifically, we find that a tilt and moving lattice applied to fermions in a kagome optical lattice results in Eq. 2 with complex hopping and staggered flux to yield $\Phi_\Delta = -\Phi_\nabla = \Phi_0/4$. We have checked that varying the angle and other parameters does not lead to a uniform flux,

though other irregular flux patterns are possible. We conclude that a method already realized in the laboratory (introducing flux in optical lattices using a tilt and a moving lattice) always leads to staggered flux patterns in kagome optical lattices.

We now conjecture on the role of strong interactions in the staggered flux case. The staggered flux ground state of Eq. 3 is argued [8] to be a gapless spin liquid where the zero-energy excitations fall along three nodal lines that all cross zero in momentum space. The gapless nodal lines are protected by symmetry but finite size effects may open a gap. We used numerical exact diagonalization on Eq. 3 with up to 18 spins with periodic boundary conditions to study the spectrum in all spin sectors. We find small gaps ($\gtrsim 0.05J_C$) at expected gapless points. We conclude that large system sizes are needed to see the degeneracy because the gapless spectrum allows strong finite size effects. Numerical work on kagome ladders with as many as 200 spins show a gap [8] that decreases linearly with system size from $\sim 0.012J_C$ for 50 spins to below $0.002J_C$ for 200 spins, thus establishing a gapless phase for large system sizes. This work also shows that the gapless phase is stable for $J_C/J_H \gtrsim 0.8$. This range corresponds to $t/U \gtrsim 2/3$ and $|\Phi_{\Delta, \nabla}| = \Phi_0/4$ in terms of Hubbard parameters, indicating that the gapless spin liquid phase is indeed reachable in a perturbative limit where t/U is still less than one. Further work would be needed to study the gapless phase for lower values of t/U , where the perturbative limit is more precise.

Discussion: Fermions in a kagome optical lattice in the Heisenberg limit can be driven into QSLs by applying fluxes that lead to chiral three-spin terms. If the final state of the combined lattice/flux system is to approximate a thermal state, we must assume that the initial state is at low enough entropies to lead to an approximation to the QSLs discussed here. The low entropy constraint is non-trivial in the context of the CSL regime. Recent work estimates that entropies per particle below $\sim 0.8k_B$ are needed to reach the Laughlin regime of bosons [57]. This estimate can serve as a benchmark for the closely related CSL. The entropy to reach the CSL is, by this measure, within reach of atomic gas microscopes [16–34] which have already realized the Heisenberg (antiferromagnetic) limit in a square optical lattice [16] with entropies per particle below $\log(2)k_B \approx 0.7k_B$.

The gapless spin liquid, by contrast, hosts a large number of (nearly) zero-energy states and may therefore offer favorable entropy requirements. The required entropy (which scales as the logarithm of the number of ground states) is not as low as the CSL. A single spin excitation along one of the degenerate nodal lines hosts an entropy per particle $\sim \log(N)/Nk_B$, for N spins. High occupancy of degenerate nodal lines implies that entropy can be large in finite sized systems. From an entropy perspective, gapless spin liquids therefore appear to be simpler to realize because the low energy manifold can be accessed at higher entropies in finite sized systems.

QSL ground states discussed here are more difficult to observe than conventionally ordered spin states because the ground states are uniform and otherwise featureless. The CSL

has chiral edge modes which could be observable using the spin analogue of recently realized quantized circular dichroism [58, 59]. Spin liquids also distinguish themselves in their fractionalized excitations. CSLs have anyon excitations which can lead to non-trivial power law behavior [35, 60] in the dynamical structure factor and can be observed with Bragg scattering [61–64]. The gapless spin liquid phase can be revealed in measures of the dynamical structure factor as excitations populate degenerate nodal lines, revealing the gapless spinon surfaces. In this paper we have constructed a route to such spin liquids in ultra-cold atom systems with short-ranged interactions to foster their identification in the laboratory.

V.W.S. acknowledges support from AFOSR (FA9550-18-1-0505). V.W.S. and S.T acknowledge support from ARO (W911NF-16-1-0182). We thank B. Bauer for helpful conversations.

* Current address: Blueshift Asset Management, 151 Bodman Pl., Suite 301, Red Bank, New Jersey 07701, United States

† Email address:scarola@vt.edu

- [1] L. Balents, *Nature* **464**, 199 (2010).
- [2] Y. Zhou, K. Kanoda, and T.-K. Ng, *Rev. Mod. Phys.* **89**, 025003 (2017).
- [3] V. Kalmeyer and R. B. Laughlin, *Phys. Rev. Lett.* **59**, 2095 (1987).
- [4] X. G. Wen, F. Wilczek, and A. Zee, *Phys. Rev. B* **39**, 11413 (1989).
- [5] X. G. Wen, *Int. J. Mod. Phys. B* **04**, 239 (1990).
- [6] B. Bauer, L. Cincio, B. P. Keller, M. Dolfi, G. Vidal, S. Trebst, and A. W. W. Ludwig, *Nat. Commun.* **5**, 1 (2014).
- [7] K. Kumar, K. Sun, and E. Fradkin, *Phys. Rev. B* **92**, 094433 (2015).
- [8] B. Bauer, B. P. Keller, S. Trebst, and A. W. W. Ludwig, *Phys. Rev. B* **99**, 035155 (2019).
- [9] R. B. Laughlin, *Phys. Rev. Lett.* **50**, 1395 (1983).
- [10] F. Wilczek, *Phys. Rev. Lett.* **49**, 957 (1982).
- [11] C. Nayak, S. H. Simon, A. Stern, M. Freedman, and S. Das Sarma, *Rev. Mod. Phys.* **80**, 1083 (2008).
- [12] I. Bloch, J. Dalibard, and W. Zwerger, *Rev. Mod. Phys.* **80**, 885 (2008).
- [13] C. Gross and I. Bloch, *Science* **357**, 995 (2017).
- [14] L. Santos, M. A. Baranov, J. I. Cirac, H. U. Everts, H. Fehrmann, and M. Lewenstein, *Phys. Rev. Lett.* **93**, 030601 (2004).
- [15] G.-B. Jo, J. Guzman, C. K. Thomas, P. Hosur, A. Vishwanath, and D. M. Stamper-Kurn, *Phys. Rev. Lett.* **108**, 045305 (2012).
- [16] A. Mazurenko, C. S. Chiu, G. Ji, M. F. Parsons, M. Kanász-Nagy, R. Schmidt, F. Grusdt, E. Demler, D. Greif, and M. Greiner, *Nature* **545**, 462 (2017).
- [17] M. G. W.S. Bakr, J.I. Gillen, A. Pend, M.E. Tai, S. Foelling, *Nature* **462**, 74 (2012).
- [18] J. F. Sherson, C. Weitenberg, M. Endres, M. Cheneau, I. Bloch, and S. Kuhr, *Nature* **467**, 68 (2010).
- [19] W. S. Bakr, A. Peng, M. E. Tai, R. Ma, J. Simon, J. I. Gillen, S. Folling, L. Pollet, and M. Greiner, *Science* **329**, 547 (2010).
- [20] M. Endres, M. Cheneau, T. Fukuhara, C. Weitenberg, P. Schauss, C. Gross, L. Mazza, M. C. Banuls, L. Pollet, I. Bloch, and S. Kuhr, *Science* **334**, 200 (2011).
- [21] C. Weitenberg, M. Endres, J. F. Sherson, M. Cheneau, P. Schau, T. Fukuhara, I. Bloch, and S. Kuhr, *Nature* **471**, 319 (2011).
- [22] R. Islam, R. Ma, P. M. Preiss, M. Eric Tai, A. Lukin, M. Rispoli, and M. Greiner, *Nature* **528**, 77 (2015).
- [23] S. Hild, T. Fukuhara, P. Schauß, J. Zeiher, M. Knap, E. Demler, I. Bloch, and C. Gross, *Phys. Rev. Lett.* **113**, 147205 (2014).
- [24] P. M. Preiss, R. Ma, M. E. Tai, J. Simon, and M. Greiner, *Phys. Rev. A* **91**, 41602 (2015).
- [25] L. W. Cheuk, M. A. Nichols, M. Okan, T. Gersdorf, V. V. Ramasesh, W. S. Bakr, T. Lompe, and M. W. Zwierlein, *Phys. Rev. Lett.* **114**, 193001 (2015).
- [26] M. F. Parsons, F. Huber, A. Mazurenko, C. S. Chiu, W. Setiawan, K. Wooley-Brown, S. Blatt, and M. Greiner, *Phys. Rev. Lett.* **114**, 213002 (2015).
- [27] E. Haller, J. Hudson, A. Kelly, D. A. Cotta, B. Peaudecerf, G. D. Bruce, and S. Kuhr, *Nat. Phys.* **11**, 738 (2015).
- [28] M. Miranda, R. Inoue, Y. Okuyama, A. Nakamoto, and M. Kozuma, *Phys. Rev. A* **91**, 63414 (2015).
- [29] R. Yamamoto, J. Kobayashi, T. Kuno, K. Kato, and Y. Takahashi, *New J. Phys.* **18**, 023016 (2016).
- [30] M. F. Parsons, A. Mazurenko, C. S. Chiu, G. Ji, D. Greif, and M. Greiner, *Science* **353**, 1253 (2016).
- [31] M. Boll, T. A. Hilker, G. Salomon, A. Omran, J. Nespolo, L. Pollet, I. Bloch, and C. Gross, *Science* **353**, 1257 (2016).
- [32] L. W. Cheuk, M. A. Nichols, K. R. Lawrence, M. Okan, H. Zhang, E. Khatami, N. Trivedi, T. Paiva, M. Rigol, and M. W. Zwierlein, *Science* **353**, 1260 (2016).
- [33] J.-y. Choi, S. Hild, J. Zeiher, P. Schauss, A. Rubio-Abadal, T. Yefsah, V. Khemani, D. A. Huse, I. Bloch, and C. Gross, *Science* **352**, 1547 (2016).
- [34] J. H. Drewes, L. A. Miller, E. Cocchi, C. F. Chan, N. Wurz, M. Gall, D. Pertot, F. Brennecke, and M. Köhl, *Phys. Rev. Lett.* **118**, 170401 (2017).
- [35] N. Y. Yao, M. P. Zaletel, D. M. Stamper-Kurn, and A. Vishwanath, *Nat. Phys.* **14**, 405 (2018).
- [36] R. A. Williams, S. Al-Assam, and C. J. Foot, *Phys. Rev. Lett.* **104**, 5 (2010).
- [37] M. Aidelsburger, M. Atala, S. Nascimbène, S. Trotzky, Y.-A. Chen, and I. Bloch, *Phys. Rev. Lett.* **107**, 255301 (2011).
- [38] N. R. Cooper, *Phys. Rev. Lett.* **106**, 175301 (2011).
- [39] K. Jiménez-García, L. J. Leblanc, R. A. Williams, M. C. Beeler, A. R. Perry, and I. B. Spielman, *Phys. Rev. Lett.* **108**, 1 (2012).
- [40] J. Struck, C. Ölschläger, M. Weinberg, P. Hauke, J. Simonet, A. Eckardt, M. Lewenstein, K. Sengstock, and P. Windpassinger, *Phys. Rev. Lett.* **108**, 225304 (2012).
- [41] P. Hauke, O. Tieleman, A. Celi, C. Ölschläger, J. Simonet, J. Struck, M. Weinberg, P. Windpassinger, K. Sengstock, M. Lewenstein, and A. Eckardt, *Phys. Rev. Lett.* **109**, 145301 (2012).
- [42] J. Struck, M. Weinberg, C. Ölschläger, P. Windpassinger, J. Simonet, K. Sengstock, R. Höppner, P. Hauke, A. Eckardt, M. Lewenstein, and L. Mathey, *Nat. Phys.* **9**, 738 (2013).
- [43] M. Aidelsburger, M. Atala, M. Lohse, J. T. Barreiro, B. Paredes, and I. Bloch, *Phys. Rev. Lett.* **111**, 185301 (2013).
- [44] H. Miyake, G. A. Siviloglou, C. J. Kennedy, W. C. Burton, and W. Ketterle, *Phys. Rev. Lett.* **111**, 185302 (2013).
- [45] G. Jotzu, M. Messer, R. Desbuquois, M. Lebrat, T. Uehlinger, D. Greif, and T. Esslinger, *Nature* **515**, 237 (2014).
- [46] D. S. Rokhsar, *Phys. Rev. Lett.* **65**, 1506 (1990).
- [47] D. Sen and R. Chitra, *Phys. Rev. B* **51**, 1922 (1995).
- [48] V. W. Scarola, K. Park, and S. Das Sarma, *Phys. Rev. Lett.* **93**, 120503 (2004).
- [49] O. I. Motrunich and M. P. A. Fisher, *Phys. Rev. B* **75**, 235116 (2007).

- [50] D. N. Sheng, O. I. Motrunich, and M. P. Fisher, *Phys. Rev. B* **79**, 1 (2009).
- [51] M. S. Block, D. N. Sheng, O. I. Motrunich, and M. P. A. Fisher, *Phys. Rev. Lett.* **106**, 157202 (2011).
- [52] H. C. Jiang, M. S. Block, R. V. Mishmash, J. R. Garrison, D. N. Sheng, O. I. Motrunich, and M. P. A. Fisher, *Nature* **493**, 39 (2013).
- [53] D. Jaksch, C. Bruder, J. I. Cirac, C. W. Gardiner, and P. Zoller, *Phys. Rev. Lett.* **81**, 3108 (1998).
- [54] A. H. MacDonald, S. M. Girvin, and D. Yoshioka, *Phys. Rev. B* **37**, 9753 (1988).
- [55] S. R. White, *Phys. Rev. Lett.* **69**, 2863 (1992).
- [56] See Supplemental Material.
- [57] P. T. Raum and V. W. Scarola, *Phys. Rev. Lett.* **118**, 115302 (2017).
- [58] D. T. Tran, A. Dauphin, A. G. Grushin, P. Zoller, and N. Goldman, *Sci. Adv.* **3**, e1701207 (2017).
- [59] L. Asteria, D. T. Tran, T. Ozawa, M. Tarnowski, B. S. Rem, N. Fläschner, K. Sengstock, N. Goldman, and C. Weitenberg, *Nat. Phys.*, 1 (2019).
- [60] S. C. Morampudi, A. M. Turner, F. Pollmann, and F. Wilczek, *Phys. Rev. Lett.* **118**, 1 (2017).
- [61] M. Weidemüller, A. Hemmerich, A. Görlitz, T. Esslinger, and T. W. Hänsch, *Phys. Rev. Lett.* **75**, 4583 (1995).
- [62] P. T. Ernst, S. Götzke, J. S. Krauser, K. Pyka, D. S. Lühmann, D. Pfannkuche, and K. Sengstock, *Nat. Phys.* **6**, 56 (2010).
- [63] R. Mottl, F. Brennecke, K. Baumann, R. Landig, T. Donner, and T. Esslinger, *Science* **336**, 1570 (2012).
- [64] R. A. Hart, P. M. Duarte, T. L. Yang, X. Liu, T. Paiva, E. Khatami, R. T. Scalettar, N. Trivedi, D. A. Huse, and R. G. Hulet, *Nature* **519**, 211 (2015).

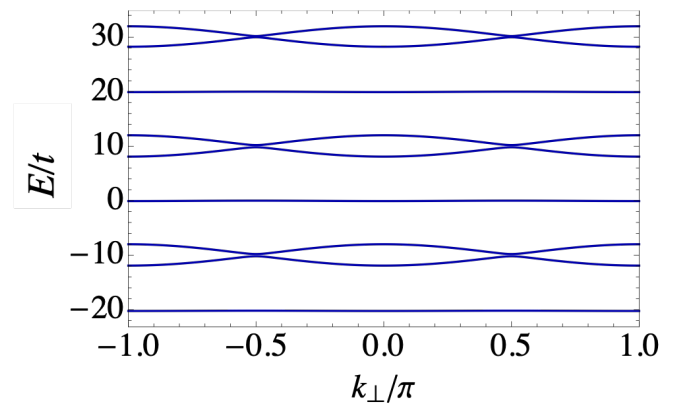


FIG. S1. Eigenvalues of the static part of Eq. 5 ($\Omega = 0$) plotted against lattice momentum perpendicular to the tilt for $\Delta = 20t$. The kagome lattice is infinite along the direction of the moving lattice but extends three unit cells along the direction of the tilt (Fig. 4). The dispersive (flat) bands define de-localized (localized) states used to vary hopping around triangles.

FLUX-DRIVEN QUANTUM SPIN LIQUIDS IN KAGOME OPTICAL LATTICES: SUPPLEMENTAL MATERIAL

Wannier-Stark States and the Effective Hamiltonian

In this section we show that Eq. 5 leads to Eq. 2 with complex hopping and effective flux. To find a parameter regime yielding an effective flux from a combination of a tilt and a moving lattice, we first study the impact of the first two terms in Eq. 5 on the basis of Wannier functions. We numerically solve for the eigen-modes for a system which is finite along the direction of tilt while infinite along the orthogonal axis. The momentum along the orthogonal axis, k_{\perp} , is a good quantum number. In the limit of strong tilt, we find two types of states plotted in Fig. S1. States localized near site \mathbf{R}_1 are dispersionless as its hopping to sites \mathbf{R}_2 and \mathbf{R}_3 (See Fig. 4) are suppressed due to the energy difference, and there is no hopping possible along the direction perpendicular to the tilt. These states appear as flat bands in Fig. S1. (This suppression of hopping is key to allowing the moving lattice to generate a complex hopping.) States localized near sites \mathbf{R}_2 and \mathbf{R}_3 can hop freely along the direction perpendicular to the tilt and therefore form the dispersive bands in Fig. S1 with bandwidth $4t$. Wannier-Stark states are then constructed from the Fourier transform of the Bloch states, where the phases are chosen to yield states maximally localized on a lattice site. We denote the Wannier-Stark states localized near \mathbf{R}_i by $|i\rangle$.

In the basis of Wannier-Stark states, the Hamiltonian in the presence of both the tilt and moving lattice becomes: $h_0^{\text{WS}} = -t \sum'_{\langle ij \rangle} |i\rangle \langle j| + \sum_i \left(\vec{\Delta} \cdot \mathbf{R}_i \right) |i\rangle \langle i| + \Omega \sum_{ij} |i\rangle \langle i| \sin(\mathbf{P} \cdot \mathbf{r} - \tau \Delta) |j\rangle \langle j|$, where the prime on the sum indicates a sum only over bonds such that $\vec{\Delta} \cdot (\mathbf{R}_i - \mathbf{R}_j) = 0$. To remove the time dependence we pass to the rotating basis, de-

finer by the unitary time evolution operator: $U = \exp \left\{ i \sum_i \left[- \left(\vec{\Delta} \cdot \mathbf{R}_i \right) \tau - F_{\mathbf{P}, \mathbf{r}} \cos(\mathbf{P} \cdot \mathbf{R}_i - \tau \Delta) \right] |i\rangle \langle i| \right\}$, where $F_{\mathbf{P}, \mathbf{r}} \equiv (\Omega/\Delta) \langle 0 | \cos \mathbf{P} \cdot \mathbf{r} | 0 \rangle$. Using U we can now remove the time dependence in h_0^{WS} using: $U^\dagger h_0^{\text{WS}} U - iU^\dagger (\partial U / \partial t)$. The resulting model is time independent but now describes dressed fermions with complex hopping, i.e, we retrieve Eq. 2. Direct numerical simulation of the Wannier functions and computation of the resulting imaginary part of the hopping shows that staggered flux with tunable strength is possible. An analytic argument for the staggered flux pattern can be derived in the weak Ω limit.

Staggered Flux in the Weak Ω Limit

In this section we show that the flux derived from Eq. 5 is staggered. We have computed this numerically in a tight-binding construction of the complex hoppings in Eq. 2. We can work in the weak Ω limit to allow analytic expressions demonstrating the mechanism behind the staggered flux. If

we let indices, 1,2, and 3 refer to the sites in upward-pointing triangle in Fig. 4 we find (for weak Ω) a complex hopping: $t_{1n} \approx \Omega \langle 1 | e^{-i\mathbf{P} \cdot \mathbf{r}} | n \rangle / (2i)$ for $n = 2, 3$, and real hopping along the remaining bond in the triangle: $t_{23} \approx t_{\mathcal{J}_0} [(2\Omega/\Delta) \sin(\mathbf{P} \cdot \mathbf{R}_{23}/2)]$. We have checked using maximally localized Wannier functions that we can maximize the flux through the plaquettes and adjust Ω to set $t = |t_{12}| = |t_{23}| = |t_{31}|$, leading to $\text{Im}[t_{12}t_{23}t_{31}] = t^3 \sin(2\pi\Phi_\Delta/\Phi_0) \approx t^3$. This shows that we can use the moving lattice to induce an effective flux in the kagome lattice.

The flux for the downward triangles is different. One can show that $t_{1n} \sim \exp[i\mathbf{P} \cdot (\mathbf{R}_1 + \mathbf{R}_n)]$ for weak Ω while t_{23} is real and the same for all triangles. This implies that the sign of the flux is the *opposite* for downward pointing triangles in comparison to upward pointing triangles in Fig. 4, i.e., $t^3 \sin(2\pi\Phi_\nabla/\Phi_0) \approx -t^3$. The change in the sign of the flux arises from the change in sign of the moving lattice potential set by \mathbf{P} . This behavior contrasts with the uniform flux realized using the same technique but in square optical lattices [43, 44].